J Biomol NMR (2009) 45:133–142
DOI 10.1007/s10858-009-9355-6

ARTICLE

Hydration dependent dynamics in RNA

Greg L. Olsen · Michael F. Bardaro Jr. · Dorothy C. Echodu · Gary P. Drobny · Gabriele Varani

Received: 12 May 2009 / Accepted: 27 June 2009 / Published online: 8 August 2009

Abstract The essential role played by local and collective motions in RNA function has led to a growing interest in the characterization of RNA dynamics. Recent investigations have revealed that even relatively simple RNAs experience complex motions over multiple time scales covering the entire ms–ps motional range. In this work, we use deuterium solid-state NMR to systematically investigate motions in HIV-1 TAR RNA as a function of hydration. We probe dynamics at three uridine residues in different structural environments ranging from helical to completely unrestrained. We observe distinct and substantial changes in ^{2}H solid-state relaxation times and lineshapes at each site as hydration levels increase. By comparing solid-state and solution state ^{13}C relaxation measurements, we establish that ns–μs motions that may be indicative of collective dynamics suddenly arise in the RNA as hydration reaches a critical point coincident with the onset of bulk hydration. Beyond that point, we observe smaller changes in relaxation rates and lineshapes in these highly hydrated solid samples, compared to the dramatic activation of motion occurring at moderate hydration.

Keywords RNA · Dynamics · Hydration · Solid state NMR · Deuterium NMR · Relaxation

G. L. Olsen · M. F. Bardaro Jr. · D. C. Echodu · G. P. Drobny (✉) · G. Varani (✉)
Department of Chemistry, University of Washington, Box 351700, Seattle, WA 98195, USA
e-mail: drobny@chem.washington.edu

G. Varani
e-mail: varani@chem.washington.edu

G. Varani
Department of Biochemistry, University of Washington, Box 357350, Seattle, WA 98195, USA

Introduction

The ability of RNA to perform its diverse functional roles frequently depends on its ability to change structure as ligands bind (Williamson 2000; Leulliot and Varani 2001). This observation suggests that many RNAs possess intrinsic dynamic features that expand their functional repertoire beyond what a static structure would otherwise allow. A well-known example of this is the HIV-1 TAR RNA (Fig. 1), one of the first systems in which the key role of large-scale conformational change for RNA function was observed (Puglisi et al. 1992; Jaeger and Tinoco 1993; Puglisi et al. 1993; Aboul-ela et al. 1995; Aboul-ela et al. 1996). TAR is a conserved stem-loop found at the 5′-end of all viral transcripts. It folds immediately after transcriptional initiation to present a structure that recruits the HIV protein Tat and the cyclin T1/cdk9 kinase complex; this complex promotes efficient transcriptional elongation (Karn 1999). Its ability to recruit these factors depends on extensive conformational changes that occur during the binding of tat protein (Puglisi et al. 1992; Puglisi et al. 1993).

Recent studies of TAR RNA have shown that the free RNA samples a wide variety of different conformations in the absence of any ligands (Al-Hashimi et al. 2002; Pitt et al. 2004; Zhang et al. 2006; Zhang et al. 2007), some of which coincide with conformations observed for TAR in various complexes with proteins and small molecules (Casiano-Negroni et al. 2007; Zhang et al. 2007). These observations strongly suggest that recognition by TAR employs a conformational capture mechanism (Williamson 2000; Leulliot and Varani 2001; Noeske et al. 2007). Therefore, motional processes in free TAR intrinsic to its sequence provide critical determinants of recognition and function.

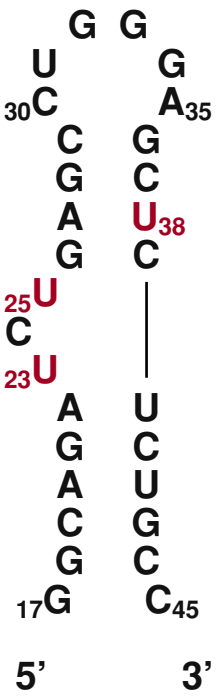

Fig. 1 Sequence and secondary structure of TAR RNA. The construct used in the present investigation contains a GAAA tetraloop in place of the apical loop; the three sites specifically deuterated for the solid state investigation (U23, U25 and U38) are identified in red

In order to further our understanding of motion-function relationships in TAR RNA, we have used both solution ^{13}C relaxation (Bardaro et al. 2009) and solid state deuterium NMR (Olsen et al. 2008) to study dynamics in TAR. The joint analysis of these two data sets provides in principle a powerful tool to study dynamics, because the two NMR techniques provide complementary information, expanding the range of observable motional timescales. However, it remains to be established whether the conditions observed in the solid state powders correspond to those present under solution conditions, particularly in regards to the local hydration. While several studies have characterized how dynamics changes in double helical DNA as a function of hydration (Kintanar et al. 1989; Alam and Drobny 1991; Tsang et al. 1992), much less is known about RNA.

In the present study, we compare dynamics in TAR RNA as monitored using ^{13}C solution relaxation methods to those observed in solid state samples under a wide range of hydration conditions from nearly dry to fully hydrated. By measuring solid state ^{2}H relaxation rates and lineshapes at three positions in TAR, U23, U25 and U38, we monitor changes in these motions as TAR progresses from low to higher levels of hydration in the solid state. Through this work, we establish conditions in the solid state that approximate those observed in solution. In addition, we study how local hydration governs motions in RNA. By comparing changes in dynamics as a function of hydration for three structurally distinct sites, we are able to observe differences in the way motional space becomes accessible to TAR as hydration progressively increases.

Materials and methods

Oligonucleotide synthesis

[5,6- ^{2}H]-labeled uridine nucleotide for deuterium dynamics experiments was prepared *in house* using well-established methods (Huang et al. 1997). Conversion of the deuterated uridine nucleotide to the phosphoramidite for subsequent incorporation into RNA samples was done by Dharmacon (Lafayette, Colorado, USA). RNA oligonucleotides were synthesized, deprotected, and desalted by Dharmacon. Each sample was checked for homogeneity using analytical denaturing polyacrylamide gel electrophoresis, and used without further purification. The following TAR RNA 29-mer constructs were used: 5′-GGC CAGA-$^{2'F}$U-CUG(pS)AGCGAAAGC*UCUCUGGCC-3′ (“U38”), 5′-GGCCAGA*U-$^{2'F}$C-UG(pS)AGCGAAAGCU CUCUGGCC-3′ (“U23”), and5′-GGCCAGA-$^{2'F}$U-C*UG (pS)AGCGAAAGCUCUCUGGCC-3′ (“U25”) where pS indicates a phosphorothioate label, -$^{2'F}$U- or -$^{2'F}$C- indicates a 2′ fluorine substitution, and *U indicates a [5,6- ^{2}H] base-labeled uridine. Previous work suggests that phosphorothioates and 2′-fluorine are non-perturbing labels (Cruse et al. 1986; Merritt et al. 1999; Olsen et al. 2005). These labels were incorporated to permit later use in structural studies of the Tat–TAR complex (Olsen et al. 2005) and to verify formation of the desired structure under solid state conditions.

Solid state NMR sample preparation

RNA oligonucleotides were dissolved in buffer (50 mM NaCl, 10 mM sodium cacodylate, pH 5.5), then frozen using liquid nitrogen and lyophilized (final composition 10% NaCl, and 4.7% cacodylate respectively, by weight upon lyophilization). To remove residual HDO and D_2O, samples were re-dissolved in deuterium-depleted water then lyophilized 3–4 times. Each sample was then re-dissolved a final time in deuterium-depleted water, annealed in a 90°C water bath for 5 min, removed from the bath and allowed to cool to room temperature for 30 min, then frozen using liquid nitrogen. All samples were then lyophilized extensively to remove residual water ($\sim$80 mtorr, 7–15 days) before transfer to the NMR sample rotor. The dry sample was packed into a 5 mm Kel-F sample chamber, and re-lyophilized to remove water absorbed during sample packing. RNA sample sizes were 5.70, 4.3, and 6.6 μmol for U38, U23, and U25 respectively.

Each RNA sample was hydrated by vapor diffusion, beginning from the dry lyophilized state, to hydration levels of 6, 9, 12, 16, 20 and 30 waters per nucleotide. Samples were hydrated in sealed chambers over saturated salt solutions containing deuterium-depleted water (Weast

1979). Water addition to the samples was monitored gravimetrically. At each hydration level used, samples were allowed to equilibrate an additional week before use in NMR experiments.

Solid-state NMR experiments

All experiments were performed on a homebuilt spectrometer (J. Gladden and G. Drobny, unpublished results) at 11.7 T field (76.76 MHz deuterium resonance frequency), using a homebuilt single-channel static deuterium probe. Pulses were generated using an American Microwave Technologies M3446 (1 kW and 10–130 MHz) amplifier. Typical 90-degree pulse times were 2.0–2.4 μs. All measurements were made at room temperature (26°C), but with continuous application of 20°C cooling air. 5 mm kel-F sample rotors were made in-house. Dwell time for all experiments was 0.2 μs and recycle delay was 1 s. Data acquisition was begun prior to the echo maximum for all experiments, and all time-domain datasets were left-shifted prior to Fourier transformation.

Deuterium lineshape data were obtained using a quadrupole echo pulse sequence (Davis et al. 1976) which used eight-step phase cycling, with an echo delay of 40 μs. Typical spectra resulted from acquisition of 300,000–500,000 scans, collected as 80,000-scan datasets that were co-added.

T_{1z} relaxation times at 76.76 MHz were determined using saturation-recovery experiments. An initial train of five 90_x pulses at 2 ms intervals was used, followed by a variable relaxation delay and quadrupole echo detection ((90°x)*n*-delay-90°x–τ–90°y–τ–echo; $n = 5$). Typical delay times for hydrated samples were 1, 100, 500, 1,000, and 2,000 ms.

T_{1Q} relaxation times were determined using the broadband Jeener–Broekaert pulse sequence (Wimperis and Bodenhausen 1986; Hoatson 1990), with eight-step phase cycling. The pulse sequence used is as follows: 90–tau1–67–tau1–45–tau2–45–[variable relaxation delay]–45–echo delay–90–echo delay–acquisition. Typical delays were 5 μs (tau1), 2.5 μs (tau2), 1, 100, 500, 1,000, and 2,000 ms (variable relaxation delay), with 40 μs echo delays.

Derivation of solid state relaxation times

Data processing was performed using in-house NMR processing software. Data were processed using 2,500 Hz line broadening prior to Fourier transformation. Powder averaged T_{1Z} and T_{1Q} relaxation times were determined using non-linear least squares fits of integrated powder spectra to a single exponential.

The solid-state ^{2}H relaxation is in general anisotropic, i.e. the components of the signal at different frequencies relax at different rates. These effects are easily observed when internal motions are fast compared to the Larmor frequency, for example in lipids, where distinct frequencies in the powder pattern correspond to distinct orientations of dynamic axes. However, for motions at or below the ^{2}H Larmor frequency, the anisotropy is small and the relationship between different frequencies in the lineshape is complex (Vold and Vold 1991). These complexities, and signal-noise limitations, preclude such a simple analysis. We nonetheless investigated this issue and failed to observe any appreciable difference in the rates of relaxation between various parts of the powder pattern. Therefore, the data were fit to a single exponential.

Solution NMR sample preparation and experiments

All solution NMR relaxation data (T_1, $T_{1\rho}$, and NOE) used in the analysis of this study have been previously reported (Bardaro et al. 2009). Data collection was performed on a Bruker Avance-500 instrument using a HCN TXI triple resonance probe at 25°C. The free TAR sample, made in house via the phage T7 RNA polymerase in vitro transcription method (Milligan et al. 1987; Milligan and Uhlenbeck 1989), was dissolved in 10 mM phosphate buffer at pH 6.6 containing 99.9% D_2O. Further details concerning T_1, $T_{1\rho}$, and NOE data collection may be found in (Bardaro et al. 2009).

Derivation of spectral density functions

Solid state spectral densities J(ω) were determined from T_{1Z} and T_{1Q} relaxation times using the following relationships:

$$R_{1Z} = \frac{1}{T_{1Z}} = \frac{3\pi^2}{2}\left(\frac{e^2qQ}{h}\right)^2 [J(\omega_o) + 4J(2\omega_o)] \quad (1)$$

$$R_{1Q} = \frac{1}{T_{1Q}} = \frac{9\pi^2}{2}\left(\frac{e^2qQ}{h}\right)^2 [J(\omega o)], \quad (2)$$

where $\left(\frac{e^2qQ}{h}\right)$ is the static quadrupolar coupling constant. A quadrupolar coupling constant (QCC) value of 179 kHz was used for all calculations in the present work (Barnes 1974; Kintanar et al. 1988, 1989). Error calculations for spectral densities assume a ±2 kHz uncertainty in static QCC values.

Spectral density analysis of ^{15}N solution NMR relaxation data follows a well established procedure (Farrow et al. 1994, 1995; Palmer et al. 1996). ^{13}C relaxation parameters were related to spectral densities (Dayie et al. 2002) by the following equations:

$$\mathrm{NOE} = 1 + \frac{d^2}{4}\left(\frac{\gamma_H}{\gamma_C}\right)[5J(1.55\omega_H)]T_1 \quad (3)$$

$$R_1 = \frac{d^2}{4}[3J(\omega_C) + 7J(1.117\omega_H)] + c^2J(\omega_C) \quad (4)$$

$$R_{1\rho} = \frac{d^2}{8}[4J(0) + 3J(\omega_C) + 13J(1.058\omega_H)] + \frac{c^2}{6}[3J(\omega_C) + 4J(0)] \quad (5)$$

$$d = \left[\frac{\mu_0 h\gamma_H\gamma_C}{8\pi^2 r_{CH}^3}\right], \quad c = \left(\frac{\omega_C}{\sqrt{3}}\right)(\Delta) \quad (6)$$

In the above equations, ω_H and ω_C are the Larmor frequencies of ^{1}H and ^{13}C respectively, μ_0 is the permeability of a vacuum, γ_H and γ_C are the gyromagnetic ratios of ^{1}H and ^{13}C, h is Planck's constant, r_{CH} is the length of the C–H bond, and Δ is the chemical shift anisotropy (CSA). The shifted ω_H values are used to correct for the effect of the $\omega = \omega_H \pm \omega_C$ terms, that were dropped in the aforementioned equations, primarily due to the difficulty of collecting data on cross-relaxation rates. If these terms were not dropped, there would be 3 observables (R_1, $R_{1\rho}$, and the NOE) from which to extract 5 unknowns (Palmer and Wagner 1992; Farrow et al. 1994; Farrow et al. 1995). Although this approach requires the assumption that $J(\omega_H) \approx J(\omega_H \pm \omega_C)$, previous studies of ^{13}C relaxation in HIV-2 TAR have shown that the reduced spectral density approach yields similar values to the complete spectral density mapping analysis (Dayie et al. 2002). Additionally, a technique formulated to improve the accuracy of the reduced spectral density analysis by calculating the upper and lower bounds at an observed frequency was adapted from ^{15}N for use on ^{13}C (Farrow et al. 1995).

For this analysis, a CSA of 212 ppm was used for C6 carbons and a bond length of 1.104 Å was assumed for all C6–H6 bonds. We assumed all chemical shift tensors are axially symmetric ($\eta = 0$) and that the axis of symmetry of the chemical shift tensor remained collinear with the C–H bond. This approximation introduces only a small error for RNAs of this size at the magnetic field employed here (Shajani and Varani 2005; Hansen and Al-Hashimi 2007).

Results

Hydration affects nucleic acid structure and dynamics. As water is introduced into solid state powder samples, it is far from clear at what level of hydration (number of water molecules per nucleotide) the conditions in a solid state powder sample approach those observed in solution. Water molecules initially populate the phosphate backbone, followed by the bases and the furanose rings (Falk et al. 1962a, b, c; Saenger 1984). Water added after completion of local hydration then contributes to bulk hydration layers surrounding the nucleic acids that progressively become closer and closer to solution conditions. At high enough water levels, macroscopic changes in the samples are apparent. The samples swell and become translucent, such that the "powder" sample is now better described as a gel. For DNA samples, these changes are apparent at a hydration level of about 12–16 waters/nucleotide. At this level of hydration, DNA internal motions become representative of those observed in solution (Alam and Drobny 1991). Below about 12 waters per nucleotide, local hydration is most likely only partially complete and some motions are quenched. For our TAR RNA samples, the visible transition of samples to a gel-like appearance is not evident until ~30 waters/nucleotide. Thus, the hydration series we report here extends well beyond what is considered sufficient to hydrate DNA to the point where the DNA internal motions are representative of solution state behavior.

Lineshapes and room temperature solid-state relaxation times for the three pyrimidine-labeled TAR bases were obtained following hydration of each sample from the dry lyophilized powder to 6, 9, 12, 16, 20 and 30 waters per nucleotide. The relaxation data for the three sites for both Zeeman and quadrupolar order decay are summarized in Fig. 2. Lineshape data for the full hydration series is presented for each of the three sites in Fig. 3. Typically, collection of these data required approximately 10–14 days per sample per hydration state; particularly at higher hydration levels, low signal/noise levels require considerable signal averaging. Despite the demand on spectrometer time, we considered this work to be necessary for any subsequent study of this RNA and to make a validated comparison with solution relaxation data.

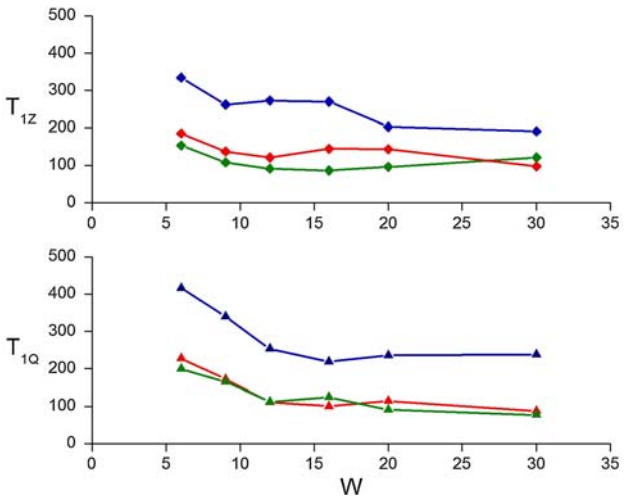

Fig. 2 ^{2}H relaxation times (T_{1z}, top and T_{1Q}, bottom, in ms) recorded in the solid state as a function of hydration levels, for the 5H, 6H positions of U38 (*blue*), U25 (*green*) and U23 (*red*)

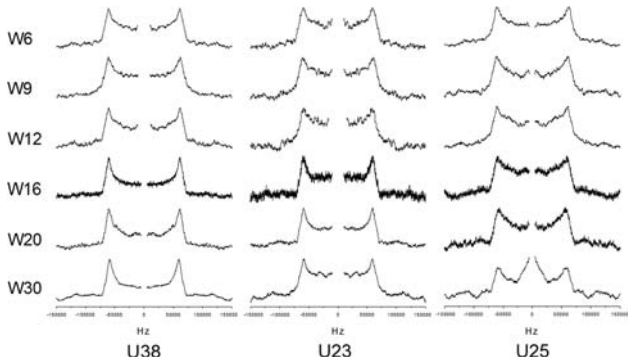

Fig. 3 Solid state lineshapes at different levels of hydration (from $W = 6$ to $W = 30$), for U38, U23, and U25. The signal in the center of the spectrum is dominated by the sharp peak corresponding to residual ^{2}H in the deuterium-depleted water, and has been removed to allow closer inspection of the data

Low hydration

At low hydration levels (6–9 waters per nucleotide, $W = 6$ and $W = 9$), hydration of the backbone should be substantial, while hydration of the bases and sugars remains incomplete. At this hydration level, the lineshapes for all three sites are consistent with the presence of only small-amplitude, fast limit or 'rigid' dynamics. However, the two single-stranded sites in TAR show markedly faster relaxation times than the base-paired residue, with T_{1Z} and T_{1Q} values for U23 and U25 both approximately half those measured for U38. Test relaxation series collected in the dry lyophilized state (data not shown) indicate that relaxation times for all three sites would likely exceed 5 s in the $W = 0$ limit, consistent with the expectation that restricted dynamics present in the dry RNAs would result in relaxation regimes on the fast side of the T_1 minimum. The much more rapid relaxation observed at $W = 6$ suggests that rehydration of the backbone results in a significant increase in conformational freedom at all sites even at this relatively low water content. Not unexpectedly, this effect is considerably more pronounced for the unpaired residues.

These results are consistent with previous deuterium solid state NMR studies showing that internal motions increase and relaxation times decrease in DNA and RNA as water is re-introduced into solid nucleic acids (Brandes et al. 1986; Brandes et al. 1988; Kintanar et al. 1989; Alam and Drobny 1991; Tsang et al. 1992; Wang et al. 1992, 1994). Interestingly, T_{1Z} for the helical residue (U38) is longer than what is typically observed for pyrimidines in DNA helices (Brandes et al. 1986; Kintanar et al. 1989), suggesting that RNA bases are more rigid than those in DNA.

Increase in hydration from 6 to 9 waters per nucleotide produced sharp decreases in both T_{1Z} and T_{1Q} values for each of the TAR residues probed (Fig. 2), likely corresponding to increases in motional amplitudes and/or decreases in rates at each of the sites, or both. This is again consistent with the expectation that under conditions of incomplete local hydration, introduction of additional water increases the local mobility.

The solid state lineshapes are a very sensitive indicator of ns–μs motions. However, despite the drop in relaxation times in going from 6 to 9 water per nucleotide, U38 does not show a marked difference in lineshape from what is in essence a static line shape at low hydration (Fig. 3); neither narrowing of the powder pattern 'horns' nor changes in the central 'wells' of the lineshapes are observed as hydration is increased from $W = 6$, through $W = 9$ to 12 for this helical residue. In contrast, U25, and to a lesser extent U23, both begin to display small lineshape modulations characteristic of motions nearer ω_Q at $W = 9$ (Figs. 4, 5). Horn narrowing with each increase in hydration is particularly clear for U25 (Figs. 4 and 5), suggesting the presence of ns–μs motions even in this semi-dry state.

Moderate hydration

The rapid decreases in T_{1Z} relaxation times seen during initial re-introduction of water to the TAR samples ceased once moderate hydration levels ($W = 12$) were reached. The studies of nucleic acid hydration in DNA cited above suggest that, following re-population of the phosphates, the bases and furanose hydration is completed at water levels $W = 12$–16. In TAR, hydration to $W = 12$ results in additional large decreases in T_{1Z} values for U23 and U25, but T_{1Z} for U38 increases only slightly from its $W = 9$ value. T_{1Q} values show sharp decreases at each position.

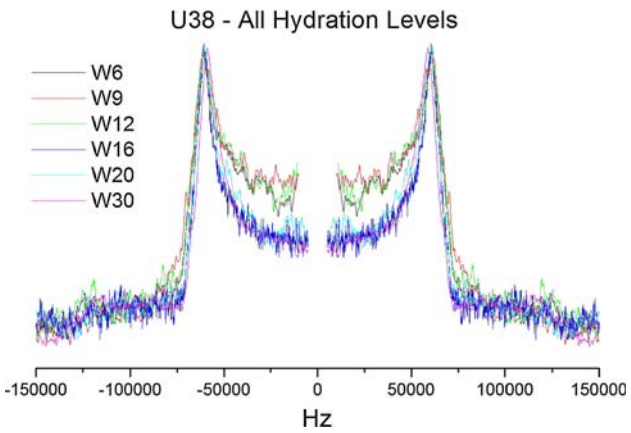

Fig. 4 Overlay of solid state lineshapes for U38 at different levels of hydration from $W = 6$ to $W = 30$. The signal in the center of the spectrum is dominated by the sharp peak corresponding to residual ^{2}H in the deuterium-depleted water, and has been removed to allow closer inspection of the data

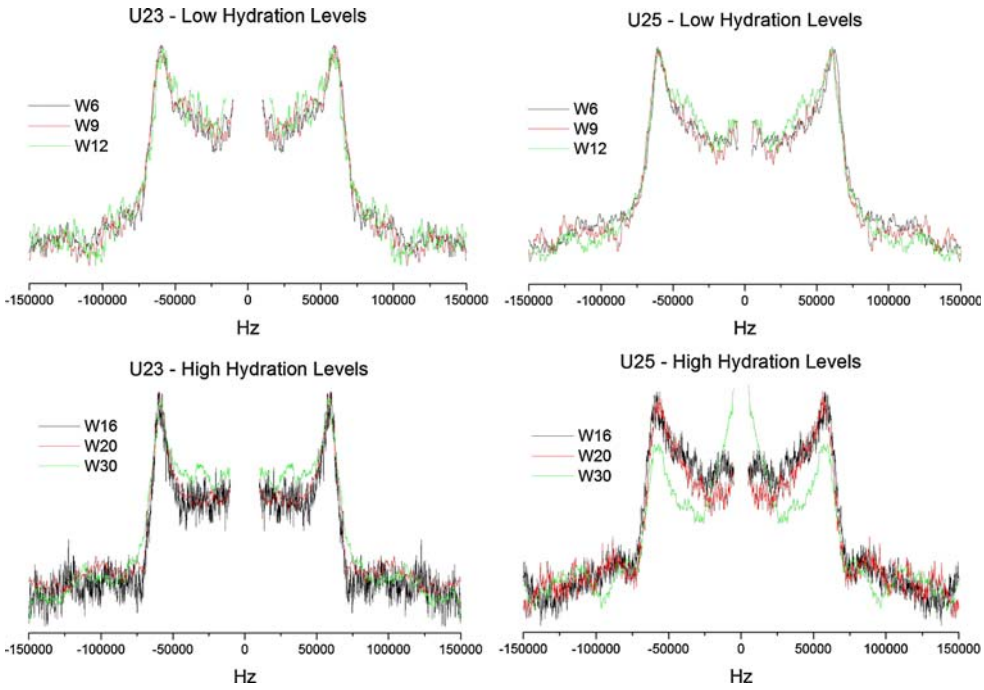

Fig. 5 Overlays of solid state lineshapes at different levels of hydration from $W = 6$ to $W = 30$, for U23 and U25. The signal in the center of the spectrum is dominated by the sharp peak corresponding to residual ^{2}H in the deuterium-depleted water, and has been removed to allow closer inspection of the data

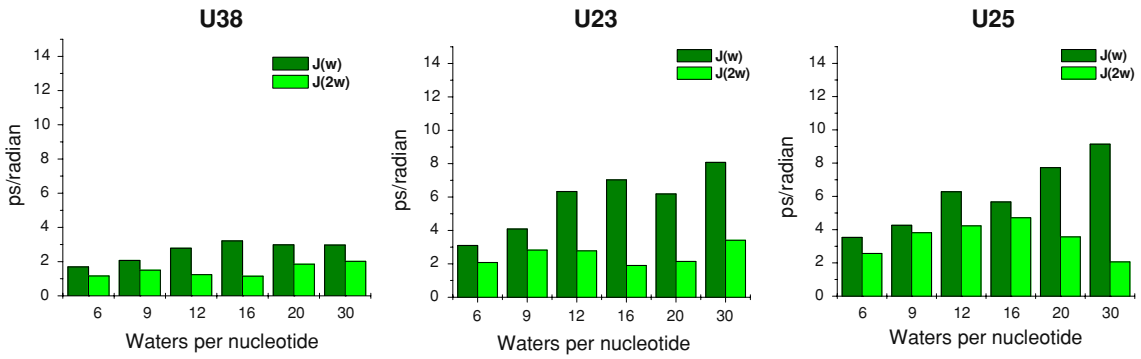

Fig. 6 Spectral density functions derived from the solid state relaxation rates as a function of sample hydration; ω_0 corresponds to 76.77 MHz

The distinct dynamic features of the three residues become more apparent upon increasing hydration to $W = 12$ (Fig. 2). This is particularly evident in the spectral densities (Fig. 6), which appear to diverge at this hydration level for the helical (U38) and single-stranded (U23 and U25) residues. The spectral densities $J(\omega_o)$ and $J(2\omega_o)$ for each of the two single-stranded residues are at least double the values for U38. The two single-stranded residues are different from each other as well. At $W = 12$, spectral density ratios $J(\omega_o)/J(2\omega_o)$ for U23 plateau at $\sim$2.5, while a continued increase in $J(2\omega_o)$ keeps the ratio near one for U25.

The lineshapes show an equally dramatic response to changes in hydration, but this occurs at $W = 16$ rather than at $W = 12$: all three lineshapes change noticeably at this hydration, with U38 showing the clearest trend. While its central well is Pake-like and essentially 'static' from $W = 6$ to $W = 12$, at $W = 16$ a pronounced drop in well amplitude is seen, indicating the onset of slower, near-μs motion in the solid state sample (Fig. 4). U23 maintains a constant horn separation throughout the hydration series, but its central well shape also changes at $W = 16$. For U25, the central well becomes markedly more angular at $W = 16$; both single-stranded sites thus clearly display modulation owing to motions in the ns–μs regime at $W = 16$.

High hydration

Studies in DNA have shown that, following hydration to about $W = 12$–16, local hydration is effectively complete. Addition of water beyond this point contributes to bulk hydration, but does not contribute further to local hydration of the bases (Saenger 1984; Alam and Drobny 1991). Hydration beyond $W = 16$ also typically results in swelling

of DNA samples. Consistent with this observation, increases in sample volume at high hydration were observed in each of the RNA samples studied here as well, although this occurred at a higher hydration level than has been observed in DNA. Figure 2 reveals that relaxation rates at each site begin to stabilize at about $W = 16$, and show only small changes in response to additional hydration. By $W = 30$, both T_{1Z} and T_{1Q} for the single-stranded residues converge to values approximately half of those seen for the helical residue U38. Intriguingly, U23 shows a small increase in the T_{1Q} relaxation time between $W = 16$ and $W = 20$, possibly reflecting structural changes or further changes in motions as hydration proceeds to $W = 20$. We note that at $W = 20$ and $W = 30$, U38 shows an increase in $J(2\omega_o)$ (Fig. 6), perhaps indicative of an onset of faster or larger-amplitude helical motions when hydration levels increase to the point that bulk hydration occurs. The U38 lineshape changes little as hydration increases beyond $W = 16$.

Also of note is the drop in $J(2\omega_o)$ at U25 beginning at $W = 20$ (Fig. 6), suggesting that motions at this site may continue to change when bulk hydration begins. Consistent with this suggestion, the lineshape for U25 shows a dramatic change at $W = 30$. The central well moves up, indicating the activation of either faster motions in the ns–μs range or of motions of larger amplitude than those observed at lower hydration.

For U23 and U38, there is a clear transition in motional regime at $W = 16$, then very similar lineshapes are maintained throughout the remainder of the hydration series. For U23, the horn width does not change at all from $W = 6$ to $W = 30$, while U38 shows only a very slight narrowing in the horns at $W = 20$ and $W = 30$, which, like the spectral density shifts at high hydration, could indicate the possible activation of faster motions of small amplitude or a larger amplitude domain motion, or both. Evidence of new motions at high hydration was observed only for U25, perhaps reflecting the lack of structural restraints on this residue.

Dynamics in the solution state

The ^{13}C solution relaxation parameters, T_1, $T_{1\rho}$, and NOE, were collected for 24 of the 29 base residues of the free TAR 29-mer, as reported recently (Bardaro et al. 2009). It was not possible to collect relaxation parameters for U25 because of spectral overlap, but data published by others (Hansen and Al-Hashimi 2007) on a similar TAR construct without spectral overlap show that C24, the base adjacent to U25, has very similar relaxation times and therefore motions to U25. Therefore, we compare the solution relaxation behavior of C24 to the solid state properties of U25. Table 1 summarizes solution relaxation data for each of the three representative sites, as well as average parameters for all 24 measured sites, for ease of comparison. Because we could find no evidence of μs–ms motions at any of the three sites, these data report primarily on ps–ns motions.

Table 1 Solution relaxation parameters for TAR RNA (Bardaro et al. 2009) for U23, C24 and U38, shown with the average C6 relaxation values for all base paired residues

	Average	U23	C24	U38
T_1 (ms)	354.6	328.2	322.5	354.1
T_{1p} (ms)	25.2	28.14	34.9	24.6
NOE	1.16	1.30	1.37	1.13
S^2	0.95	0.84	0.70	0.96

The relaxation data for U23 indicate that its base experiences limited ps–ns motions. The model-free analysis shows it has a moderately low order parameter $S^2 = 0.84$, compared to the average of helical bases at 0.95. The base of C24, next to U25 in the single-stranded bulge region, appears to undergo more significant ps–ns motions, indicated by the T_1, T_{1p}, and NOE ratio, as well as a lower order parameter of 0.7. Relaxation parameters for the base of U38 (Table 1) demonstrate a lack of substantial ps–ns motions. The model-free analysis shows that it has a high order parameter of 0.96, while the average for helical bases is 0.95.

Discussion

The application of residual dipolar couplings and solid state deuterium NMR to studies of TAR dynamics has revealed that TAR is motionally rich within the ns–μs timescale (Hansen and Al-Hashimi 2007; Zhang et al. 2007; Olsen et al. 2008). Solid state deuterium NMR has a unique ability to probe this ns–μs motional regime, while solution relaxation experiments contain motional information only on dynamics occurring at rates faster than the global tumbling (Palmer et al. 1996; Palmer 2001, 2004; Shajani and Varani 2005, 2007) or much slower motions when the lineshape is modulated by chemical exchange (Korzhnev et al. 2002; Kempf and Loria 2003; Shajani and Varani 2007). Thus, when integrated together, the two techniques can probe the entire ps–ms motional range. However, such integration requires knowledge that the structure and internal dynamics in the solid state powder and in solution are the same. We have previously established that TAR adopts similar structures in solution and the solid state (Olsen et al. 2005). A second equally important issue is whether dynamics in a hydrated solid approaches the behavior observed in a liquid.

In this study, we also wished to investigate the pathways by which this RNA accesses available motional space as it progresses from a dry lyophilized state to the fully hydrated form observed under solution conditions. Monitoring of relaxation behavior as a function of hydration level permits investigation of dynamic responses to localized changes in conformational freedom as the RNA rehydrates from the relatively dry state found at low hydration levels (6–9 water molecules per nucleotides) to conditions of higher hydration (>12–16 waters per nucleotide) where even the macroscopic appearance of the solid state sample changes to induce a gel-like appearance. Based on studies conducted with DNA (Kintanar et al. 1989; Alam and Drobny 1991), our expectation was that motions should become close to those observed in solution in the high water limit, once local hydration is complete and bulk hydration has relaxed restraints on collective motions. Two deuterium NMR investigations have been conducted over a decade ago on RNA dynamics in the solid state. However, neither studied specific sites since both examined uniformly purine-labeled helical sites (Tsang et al. 1992; Wang et al. 1992; Wang et al. 1994). Nevertheless, these studies did reveal intriguing differences between base dynamics in RNA helices and their DNA counterparts. At low water content, the DNA bases at helical sites relaxed much faster than bases in an RNA helix with identical sequence, suggesting that RNA base pairs are initially more rigid than in DNA. As water increased, however, the two behaviors converged. To date there has been no systematic study of site-specific of RNA dynamics for either single- or double-stranded nucleotides, as a function of hydration in the solid state.

We have observed that all three sites we have investigated (U23, U25 and U38) show essentially static lineshapes at low hydration ($W = 6$), suggesting that ns–μs motions are essentially frozen at low water content (though not the faster motions observed by relaxation methods, as discussed below). At intermediate hydration (between $W = 9$ and $W = 16$,) the lineshapes only change significantly for the most mobile and solvent accessible of the two single-stranded nucleotides, U25 (horn narrowing). However, at W = 16 noticeable changes in lineshapes suddenly occur at all three sites, consistent with the onset of ns–μs motions as hydration increases from 12 to 16 water per nucleotides. At each site, the behavior of both relaxation rates converges in the high hydration limit (above $W = 16$), most clearly for the helical site, U38. This is accompanied by correspondingly smaller changes in the lineshapes in the highly hydrated solid samples, compared to the dramatic activation of motions that we see between $W = 12$ and $W = 16$. Beyond this hydration level, only the U25 lineshape changes significantly as more waters are added.

The relaxation data indicate that helical residue U38 occupies a motional regime that is quite distinct from that of the two extrahelical residues, U23 and U25, as evidenced by consistently higher T_{1Z} and T_{1Q} values (Fig. 2). These markedly higher relaxation times suggest that U38 is considerably more rigid than either single stranded nucleotide at low levels of hydration. The addition of water molecules lowers relaxation times, indicating increased flexibility, yet the U38 base remains much more rigid than U25 and U23 at all hydration levels. These results are in good agreement with what is observed in solution (Bardaro et al. 2009), where U38 is more rigid on the time scale sampled by solution relaxation methods (faster than about 10 ns). The solution relaxation data (T_1, $T_{1\rho}$, and NOE) confirm that U38 is *not* experiencing any significant ps–ns motion (Bardaro et al. 2009) in solution; its high order parameter also indicates significant motional rigidity. This trend is also reflected in the consistently lower spectral density values ($J(\omega_o)$ and $J(2\omega_o)$, where ω_o is 77 MHz), which show only small increases as a function of hydration (Fig. 6).

In contrast to the conclusions of solution studies, the solid state NMR lineshapes indicate that U38 is motionally active on a longer timescale than that visible to solution methods (Olsen et al. 2008). In fact, the U38 lineshape hydration series shows a particularly clear and sudden onset of these slow (ns–μs) motions at $W = 16$ (Fig. 3). Remarkably, the lineshape then remains consistent throughout the rest of the hydration series. The absence of significant horn narrowing at higher hydration suggests that the new motions which appear at $W = 16$ are either slow or small in amplitude, and the decrease in well amplitude indicates that the motions must be in the μs regime or slower. Taken together with the solution relaxation data (Bardaro et al. 2009), the lineshape and solids relaxation data are consistent with the presence of the slow (μs) collective dynamics in TAR that may coincide with those revealed by RDC studies in solution (Al-Hashimi et al. 2002; Pitt et al. 2004; Zhang et al. 2007).

As expected from their structure, both U23 and U25 are more mobile than U38, exhibiting fast ps–ns motions in solution as well as slower ns–μs motions in the solid. The solid state relaxation data show that both residues have consistently lower T_{1Z} and T_{1Q} values compared to U38 (Fig. 2), and that, at most hydration levels, U23 exhibits slightly higher T_{1Z} and T_{1Q} values than U25. Unlike U38, the relaxation times for U23 and U25 continue to change until $W = 30$, the highest hydration level probed. Interestingly, both $J(\omega_o)$ and $J(2\omega_o)$ for U23 increase as a function of hydration (Fig. 6), indicating an increase in motional amplitude and/or rates; for U25, only $J(\omega_o)$ increases with hydration.

The lineshapes of U23 and U25 also respond differently to hydration. U23 shows only small reductions in horn width from $W = 6$ to $W = 30$. In contrast, narrowing of the U25 horns occurs with each successive increase in hydration, reflecting increases in motional amplitudes or, in a regime below ω_Q, increases in rates. However, more specific conclusions concerning these changes would require modeling of the data. Since U25 is unrestrained in the structure, its apparent motional richness is to be expected. The solution relaxation data on the adjacent base C24, together with the dramatic lineshape modulation at increasing hydration, point either to the progressive emergence of faster motions or of larger-amplitude motions as hydration increases; it is not clear whether this process is fully completed even at the highest water content we have investigated. In contrast, the U23 lineshape does not change significantly after $W = 16$, although its spectral densities continue to increase. Thus, for all three sites, ns–μs motions are activated by $W = 16$, and then do not change significantly for two of the three sites probed throughout the rest of the hydration series. This conclusion is consistent with the solution relaxation data as well which, while insensitive to ns–μs motions, show no signs of slower motions in the μs–ms range at any of the three sites. These results suggest that the majority of slower collective motions are already present in the RNA by $W = 16$.

Conclusions

We have studied the hydration dependence of the motions of three bases in TAR RNA, representing helical, partially restrained, and fully single-stranded nucleotides in the molecule, by systematically recording solid state deuterium NMR lineshapes and relaxation times as a function of hydration and comparing these results with solution relaxation measurements. We have found that all three sites show dramatic and sudden changes in the lineshapes at intermediate hydration levels coincident with initiation of bulk hydration, indicating the onset of ns–μs motions. Beyond this point, changes in lineshape and relaxation times are more subtle, except for U25, as hydration continues to increase and motions converge towards those observed in the liquid state. Only for U25, which experiences dramatic changes in conformation as the TAR structure changes upon binding of Tat protein and small molecule ligands (Aboul-ela et al. 1995; Aboul-ela and Varani 1998), do significant changes in dynamics continue throughout the entire hydration series.

The importance of intermediate motions to RNA function makes it increasingly clear that a full integration of solution and solid state NMR will be crucial for a comprehensive description of the complex atomic motions that underlie its biological function. The present work establishes conditions where this integration can be pursued, and reveals that the transition in RNA dynamics that activates intermediate time scale motions occurs suddenly as hydration reaches a critical point coincident with bulk hydration. It is probable that this transition coincides with the onset of collective motions in the RNA observed in solution by residual dipolar couplings.

Acknowledgements We thank professors J Michael Schurr and Bruce Robinson for helpful discussions of hydration and interpretation of relaxation data. This work was supported by a grant from the NSF MCB 0642253.

References

Aboul-ela F, Varani G (1998) Recognition of HIV-1 TAR RNA by tat protein and tat-derived peptides. J Mol Struct 423:29–39

Aboul-ela F, Karn J, Varani G (1995) The structure of the human immunodeficiency virus type-1 TAR RNA reveals principles of RNA recognition by Tat protein. J Mol Biol 253(2):313–332

Aboul-ela F, Karn J, Varani G (1996) Structure of HIV-1 TAR RNA in the absence of ligands reveals a novel conformation of the trinucleotide bulge. Nucleic Acids Res 24(20):3974–3981

Alam TM, Drobny GP (1991) Solid-state NMR studies of DNA structure and dynamics. Chem Rev 91:1545–1590

Al-Hashimi HM, Gosser Y, Gorin A, Hu W, Majumdar A, Patel DJ (2002) Concerted motions in HIV-1 TAR RNA may allow access to bound state conformations: RNA dynamics from NMR residual dipolar couplings. J Mol Biol 315:95–102

Bardaro MF Jr, Shajani Z, Patora-Komisarska K, Robinson JA, Varani G (2009) How binding of small molecule and peptide ligands to HIV-1 TAR alters the RNA motional landscape. Nucleic Acids Res 37:1529–1540

Barnes RG (ed) (1974) In advances in nuclear quadrupole resonance. New York

Brandes R, Vold RR, Vold RL, Kearns DR (1986) Effects of hydration on purine motion in solid DNA. Biochemistry 25:7744–7751

Brandes R, Vold RR, Kearns DR, Rupprecht A (1988) A 2H-NMR study of the A-DNA conformation in films of oriented Na-DNA: evidence of a disordered B-DNA contribution. Biopolymers 27:1159–1170

Casiano-Negroni A, Sun X, Al-Hashimi HM (2007) Probing $Na^{(+)}$-induced changes in the HIV-1 TAR conformational dynamics using NMR residual dipolar couplings: new insights into the role of counterions and electrostatic interactions in adaptive recognition. Biochemistry 46:6525–6535

Cruse WBT, Salisbury SA, Brown T, Cosstick R, Eckstein F, Kennard O (1986) Chiral phosphorothioate analogues of B-DNA. The crystal structure of Rp-dGp(S)CpGp(S)CpGp(S)C. J Mol Biol 192:891–905

Davis JH, Jeffrey KR, Bloom M, Valic MI, Higgs TP (1976) Quadrupolar echo deuteron magnetic resonance spectroscopy in ordered hydrocarbon chains. Chem Phys Lett 42:390–394

Dayie KT, Brodsky AS, Williamson JR (2002) Base flexibility in HIV-2 TAR RNA mapped by solution ^{15}N, ^{13}C NMR relaxation. J Mol Biol 317:263–278

Falk M, Hartman KA, Lord RC (1962a) Hydration of deoxyribonucleic acid. I. a gravimetric study. J Am Chem Soc 84:3843–3846

Falk M, Hartman KA, Lord RC (1962b) Hydration of deoxyribonucleic acid. II. An infrared study. J Am Chem Soc 85:387–391

Falk M, Hartman KA, Lord RC (1962c) Hydration of deoxyribonucleic acid. III. A spectroscopic study of the effect of hydration on the structure of deoxyribonucleic acid. J Am Chem Soc 85:391–394

Farrow NA, Muhandiram DR, Singer AU, Pascal SM, Kay CM, Gish G, Shoelson SE, Pawson T, Forman-Kay JD, Kay LE (1994) Backbone dynamics of a free and a phosphopeptide-complexed Src homology 2 domain studied by 15N NMR relaxation. Biochemistry 33:5984–6003

Farrow AN, Zhang O, Szabo A, Torchia DA, Kay LE (1995) Spectral density function mapping using 15N relaxation data exclusively. J Biomol NMR 6:153–162

Hansen AL, Al-Hashimi HM (2007) RNA dynamics by carbon relaxation and domain elongation. J Am Chem Soc 129:16072–16082

Hoatson GL (1990) Broadband composite excitation sequences for creating quadrupolar order in 2H NMR. J Magn Reson 94:152–159

Huang X, Yu P, LeProust E, Gao X (1997) An effficient and economic site-specific deuteration strategy for NMR studies of homologous oligonucleotide repeat sequences. Nucleic Acids Res 25:4758–4763

Jaeger JA, Tinoco I Jr (1993) An NMR study of the HIV-1 TAR element hairpin. Biochemistry 32:12522–12530

Karn J (1999) Tackling tat. J Mol Biol 293:235–254

Kempf GJ, Loria JP (2003) Protein dynamics from solution NMR. Cell Biochem Biophys 37:187–211

Kintanar A, Alam TM, Huang W, Schindele DC, Wemmer DE, Drobny GP (1988) Solid-state 2H NMR investigation of internal motion. J Am Chem Soc 110:6367–6372

Kintanar A, Huang WC, Schindele DC, Wemmer DE, Drobny GP (1989) Dynamics of bases in hydrated $[d(CGCGAATTCGCG)]_2$. Biochemistry 28:282–293

Korzhnev DM, Skrynnikov NR, Millet O, Torchia DA, Kay LE (2002) An NMR experiment for the accurate measurement of heteronuclear spin-lock relaxation rates. J Am Chem Soc 124:10743–10753

Leulliot N, Varani G (2001) Current topics in RNA-protein recognition: control of specificity and biological function through induced fit and conformational capture. Biochemistry 40(27):7947–7956

Merritt ME, Sigurdsson ST, Drobny GP (1999) Long-range measurements to the phosphodiester backbone of solid nucleic acids using 31P–19F REDOR NMR. J Am Chem Soc 121:6070–6071

Milligan JF, Uhlenbeck OC (1989) Synthesis of small RNAs using T7 RNA polymerase and synthetic DNA templates. Methods Enzymol 180:51–62

Milligan JF, Groebe DR, Witherell WG, Uhlenbeck OC (1987) Oligoribonucleotide synthesis using T7 RNA polymerase and synthetic DNA templates. Nucleic Acids Res 15:8783–8798

Noeske J, Buck J, Furtig B, Nasiri HR, Schwalbe H, Wohnert J (2007) Interplay of 'Induced Fit' and preorganization in the ligand induced folding of the aptamer domain of the guanine binding riboswitch. Nucleic Acids Res 35:572–583

Olsen GL, Edwards TE, Deka P, Varani G, Sigurdsson ST, Drobny GP (2005) Monitoring tat peptide binding to TAR RNA by solid-state 31P–19F REDOR NMR. Nucleic Acids Res 33(11):3447–3454

Olsen GL, Echodu DC, Shajani Z, Bardaro MF Jr, Varani G, Drobny GP (2008) Solid-state deuterium NMR studies reveal micros-ns motions in the HIV-1 transactivation response RNA recognition site. J Am Chem Soc 10:2896–2897

Palmer AGIII (2001) NMR probes of molecular dynamics: overview and comparison with other techniques. Annu Rev Biophys Biomol Struct 30:129–155

Palmer AGIII (2004) NMR characterization of the dynamics of biomacromolecules. Chem Rev 104:3623–3640

Palmer AGIII, Wagner G (1992) Mapping of spectral density functions using heteronuclear NMR relaxation experiments. J Magn Res 98:308–332

Palmer AGIII, Williams J, McDermott A (1996) Nuclear magnetic resonance studies of biopolymer dynamics. J Phys Chem 100:13293–13310

Pitt SW, Majumdar A, Serganov A, Patel DJ, Al-Hashimi HM (2004) Argininamide binding arrests global motions in HIV-1 TAR RNA: comparison with Mg^{+2}-induced conformational stabilization. J Mol Biol 338:7–16

Puglisi JD, Tan R, Calnan BJ, Frankel AD, Williamson JR (1992) Conformation of the TAR RNA-arginine complex by NMR spectroscopy. Science 257:76–80

Puglisi JD, Chen L, Frankel AD, Williamson JR (1993) Role of RNA structure in arginine recognition of TAR RNA. PNAS 90(8):3680–3684

Saenger W (1984) Principles of nucleic acid structure. Springer, New York

Shajani Z, Varani G (2005) 13C NMR relaxation studies of RNA base and ribose nuclei reveal a complex pattern of motions in the RNA binding site for human U1A protein. J Mol Biol 349(4):699–715

Shajani Z, Varani G (2007) NMR studies of dynamics in RNA and DNA by ^{13}C relaxation. Biopolymers 86:348–359

Tsang P, Kearns KR, Vold RR (1992) Deuterium quadrupole echo NMR spectra and spin-lattice relaxation of synthetic polyribonucleotides. J Am Chem Soc 114:6585–6587

Vold RR, Vold RL (1991) Deuterium relaxation in molecular solids. Adv Magn Opt Reson 16:85–171

Wang AC, Kennedy MA, Reid BR, Drobny GP (1992) A solid-state 2H NMR relaxation study of a 12 base pair RNA duplex. J Am Chem Soc 114:6583–6585

Wang AC, Kennedy MA, Reid DR, Drobny GP (1994) A solid-state 2H NMR investigation of purine motion in a 12-base-pair RNA duplex. Journal of Magnetic Resonance B 105:1–10

Weast RC (1979) Handbook of chemistry and physics. CRC Press, Boca Raton

Williamson JR (2000) Induced-fit in RNA-protein recognition. Nature Struct Biol 7:834–837

Wimperis S, Bodenhausen G (1986) Broadband excitation of quadrupolar order by modified Jeener-Broekaert sequences. Chem Phys Lett 132:194–199

Zhang Q, Sun X, Watt ED, Al-Hashimi HM (2006) Resolving the motional modes that code for RNA adaption. Science 311:653–656

Zhang Q, Stelzer AC, Fisher CK, Al-Hashimi HM (2007) Visualizing spatially correlated dynamics that directs RNA conformational transitions. Nature 450:1263–1268